JOURNAL OF SPACECRAFT AND ROCKETS
Vol. 44, No. 2, March–April 2007

Satellite Formation Mission Optimization with a Multi-Impulse Design

Aaron B. Hoskins* and Ella M. Atkins†
University of Michigan, Ann Arbor, Michigan 48105

DOI: 10.2514/1.19984

Satellite formation flight has emerged as a method to increase science return and enable missions that had been impossible with a single spacecraft. Formations often must maintain a precise geometry, which complicates mission design, given natural orbit dynamics. This paper presents a multi-impulse formation design strategy that is a compromise between active control and drift solutions. This design formulation is applied to optimize the magnetospheric multiscale tetrahedron mission using two optimization algorithms, a hierarchical strategy, and a particle swarm approach. Results are presented for a variety of multi-impulse problem specifications, including formation attitude, demonstrating that a multi-impulse solution is a viable strategy that can dramatically improve formation accuracy and longevity at minimal fuel cost. The impact of perturbing forces on optimal designs and their costs is also characterized.

Nomenclature

a = semimajor axis of the T frame, km
c = constant coefficient to determine weight of cognitive c_1 and social c_2 influence
D = amount of delay after firing thrusters before data can be collected, s
e = eccentricity of the T frame
$\boldsymbol{g}_{\mathbf{best}}$ = vector location and cost of best candidate solution so far investigated by any particle
i = inclination of the T frame, rad
J = value of the cost function
$\boldsymbol{L}$ = tetrahedron vertices vector (L_1, L_2, L_3, and L_4)
n = number of design variables, number of orbits
$\boldsymbol{p}_{\mathbf{best},i}$ = vector location and cost of best candidate solution investigated by a specific particle
P_i = position of impulsive thruster firing ($i = 1, 2$)
$P^A_{2,j}$ = actual position of satellite j when the virtual satellite is at location P_2 ($j = 1, \ldots, 4$), km
$P^D_{2,j}$ = desired position of satellite j when the virtual satellite is at location P_2 ($j = 1, \ldots, 4$), km
$P^*_{2,j}$ = correct position of satellite j when the virtual satellite is at location P_2 ($j = 1, \ldots, 4$), km
$Q\,\mathrm{d}t$ = integrated quality factor, s
Q_G = Glassmeier quality factor
Q_R = Robert–Roux tetrahedron quality factor (1 = regular tetrahedron)
r_i = random number to vary search ($i = 1, 2$)
R_{ij} = Euler rotation angles ($i = x, y, z$ and $j = 1, 2$), rad
T_{obs} = observation time, s
$\mathbf{v}$ = velocity of a particle for the particle swarm optimization algorithm
w = weights applied to the terms of the cost function
$\mathbf{x}$ = position of a particle for the particle swarm optimization algorithm
ΔP_{2j} = difference between $P2$, j^D, and $P^A_{2,j}$, km
Δr = two-norm magnitude of Δx, Δy, and Δz, km
Δt = time step, s
ΔV = velocity change used as a measure of fuel used, km/s
ΔV_x = velocity change along the inertial x axis, km/s
ΔV_y = velocity change along the inertial y axis, km/s
ΔV_z = velocity change along the inertial z axis, km/s
Δx = position error along the inertial x axis, km
Δy = position error along the inertial y axis, km
Δz = position error along the inertial z axis, km
$\Delta\nu$ = angle between burn application sites, rad
ν_c = angle from perigee to the center of $\Delta\nu$, rad
ω = inertial weight factor to determine the influence of the current state on the next state
$\tilde{\omega}_{\mathrm{true}}$ = true longitude of periapsis of the T frame

Introduction

MISSION designs for satellite formations in orbit are typically categorized as either *natural* or *actively controlled*. Natural formations capitalize on the motion of spacecraft under central body gravitational forces to maintain certain geometries for at least a segment of a circular or elliptical orbit. The satellites in these formations do not use propellants to control their positions, except for a very occasional burn to correct orbit degradation. Actively controlled formations are those in which individual satellites are expected to apply thruster forces to maintain a prescribed geometry through active three- or six-degree-of-freedom (DOF) control. The primary design goal for actively controlled formations is to avoid costly propellant usage while meeting formation geometric constraints, a challenging task for Earth-orbiting formations.

In an early version of formation flight, Gemini 6 and 7 occupied approximately the same orbit to achieve low-fuel rendezvous. EO-1 and LandSat-7 successfully demonstrated the concept of formation flight with leader and follower, in which the follower automatically computes burns to maintain the designated separation [1]. A variety of natural orbit formation solutions have been proposed, with corrective burns applied infrequently to realign the satellite group [2–5]. In addition, analytical solutions have been published that use one burn per orbit to allow a satellite formation to occupy prescribed relative positions at the end of each orbit [6]. The concept of a virtual structure [7], virtual satellite [8], or virtual rigid body (VRB) [9,10] has been developed to facilitate actively controlled formation design and management, particularly, when high-precision geometries must be maintained. With such a representation, each spacecraft acts as a "node" in an overall formation "structure" held together by natural and active control forces rather than by rigid physical components. In

Presented as Paper 5835 at the AIAA Guidance, Navigation, and Control Conference, San Francisco, CA, 15–18 August 2005; received 9 September 2005; revision received 1 December 2006; accepted for publication 1 December 2006.

*Graduate Research Assistant, Aerospace Engineering Department. Member AIAA.
†Associate Professor, Aerospace Engineering Department. Associate Fellow AIAA.

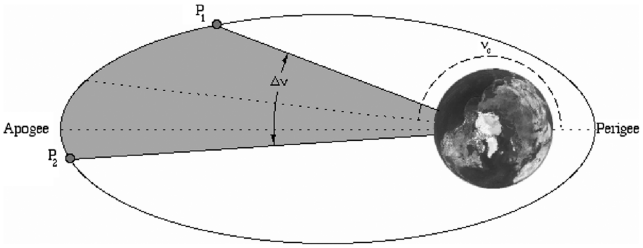

Fig. 1 Impulsive burn orbital stations.

the work of Chavez-Clemente and Atkins [10] with the VRB concept, missions were designed such that the formation actively maintained perfect geometry over a particular region of each orbit, designated by width $\Delta\nu$ and center position ν_c, as shown in Fig. 1.

Although VRB designs enable perfect geometry over an extended portion of each orbit, the use of continuous active thrust remains controversial. Current operational protocols require substantial mission support personnel whenever spacecraft burns are executed. Additionally, thruster emissions may compromise data from sensitive science instruments. The objective of this research is to investigate a novel satellite formation mission design strategy that maximizes geometric quality through the use of planned impulsive thrust commands. With this multi-impulse design strategy, impulses are applied to initiate orbits that maximize future formation quality and minimize fuel use over all required impulses. The distinction of this work is that we actively optimize impulse application as part of the mission planning process, as opposed to designing the best possible natural formation and then applying impulses when necessary to correct for perturbations. Our hypothesis is that the opportune application of low-magnitude impulses can improve overall science data quality (formation geometry) with acceptable fuel use.

The multi-impulse design strategy is applied to the Magnetospheric Multiscale (MMS) mission, a tetrahedral four-satellite formation in a highly elliptical orbit [11–14]. Following a description of the MMS multi-impulse mission design problem, we present two algorithms that were tasked with MMS optimization: a hierarchical method used in our previous work and a particle swarm approach. The results presented in this paper use optimization to solve two problems. The first is a multi-impulse solution presented as a compromise between natural orbit and VRB solutions. For the first investigation, impulse application sites and 3-D formation offset from a mission reference orbit are the design variables. The formation is not required to have a specific attitude as it acquires data. Thus, as a next step, we extend the design vector to also optimize over formation (tetrahedron) attitude. Note that in this work, the individual satellite attitudes are not considered during mission design; the term *formation attitude* is used to define the overall orientation of the aggregate tetrahedron with respect to the inertial frame. This use of *attitude* is slightly different from the more common definition that refers to individual satellite orientations.

Because of computational complexity issues, we use a purely Keplerian two-body model of dynamics for our optimization processes. Previous research has investigated the long-term influence that perturbations can have on a mission [15], and other research has investigated the creation of a state transition matrix that includes J_2 [16]. Linearized equations of motion that include J_2 have been developed [17]. However, the orbit investigated for this research has high altitude and high eccentricity, and so inclusion of additional perturbing forces is required to achieve an accurate solution. A simulator with perturbations is incorporated into the final stage of our mission design process. This paper derives perturbed solutions from the optimal Keplerian design vectors and compares their fuel use and geometric quality with the original Keplerian results.

MMS Problem Formulation

To define the multi-impulse optimization design vector, a series of reference frames that are analogous to those defining a VRB are used. First, an inertial frame is placed at the center of the Earth. The x axis points to the vernal equinox, and the z axis points to the North Pole. A target (T) frame is assigned a natural orbit defined by orbital elements a, e, i, $\tilde{\omega}_{\text{true}}$, and ν. For this paper, the T frame is assigned an equatorial orbit. The right ascension of the ascending node is therefore not defined, and that angle is combined with the argument of perigee to create the true longitude of perigee, $\tilde{\omega}_{\text{true}}$. The T frame has the same attitude as the initial inertial frame. The final reference frame, the vehicle (V) frame, has its center offset from T by the vector $\boldsymbol{V}$ that consists of the terms V_x, V_y, and V_z and is aligned in attitude with T. The V frame is constantly offset from the T frame by the vector $\boldsymbol{V}$; however, the reference frames are only used when the locations of the satellites are constrained.

The problem formulation presumes regular tetrahedron geometry, with a satellite occupying each vertex node. The distance between each of the satellites is 10 km, one of the sizes specified for MMS. As shown in Fig. 2, the formation is oriented so that the location of vertex L_1 is on the y axis of the V frame. L_2 and L_3 are equidistant from the center of the V frame parallel to the x axis, and L_4 is located on the V-frame z axis.

The following assumptions were made for all formation optimization processes:

1) Satellite motion is only influenced by Keplerian two-body forces. Although perturbing forces will vary satellite motions, general trends will remain unchanged and the inclusion of perturbing forces makes optimization intractable. Differences between the Keplerian solution and the equivalent solution simulated under a more complete force set are presented to quantify the effect of this assumption for our MMS designs.

2) Instantaneous ΔV is possible. This assumption allows us to use Lambert's solution to calculate the ΔV needed to travel between P_1 and P_2.

3) Thrust is possible in any direction at any time without the need to reorient the satellite.

4) If the calculated Robert–Roux quality factor [18] value is above 0.7, then data can be collected. Otherwise, no data can be collected. The Robert–Roux quality factor is the sole measure of tetrahedron quality for this work, functioning similarly to comparable measures such as the Glassmeier parameter [18].

5) The formation returns to the P_1 location for the next orbit.

Orbital elements for the reference T frame were defined in accordance with MMS mission specifications [13] and were presumed the same for each optimization result presented in this paper. The semimajor axis is 61,230.144 km, the eccentricity is 0.875, and, as was mentioned above, the inclination is set to zero deg. All design problems required optimization over parameters $\tilde{\omega}_{\text{true}}$, V_x, V_y, and V_z. In addition, optimal values for $\Delta\nu$ and ν_c (Fig. 1) were identified, defining the orbit reference locations at which burns P_1 and P_2 are applied.

Symmetries were identified to minimize design variable search spaces $\Delta\nu$ and ν_c, which each ranged from 0–180 deg; $\tilde{\omega}_{\text{true}}$ also originally ranged from 0–180 deg, but was readjusted to ± 30 deg range for some of the solutions presented in this paper. With the constant tetrahedron orientation presumed for this work, a $\tilde{\omega}_{\text{true}}$ rotation of 60_deg changes the apparent locations of the in-plane satellites (L_1, L_2, and L_3, as shown in Fig. 2).

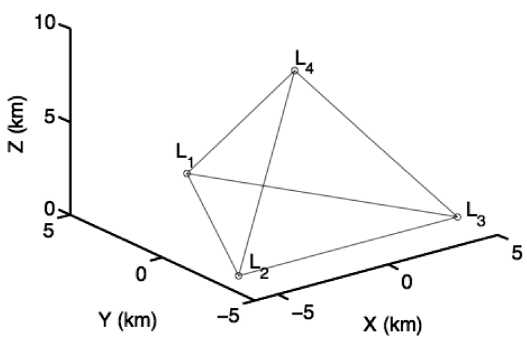

Fig. 2 Satellite offsets from the V frame.

All design problems presume all four satellites start in the Fig. 2 configuration at orbital station P_1, with the same velocity as the T frame. The satellites are constrained to be in the same configuration when the T frame reaches P_2, with velocities again matching the T-frame velocity. To achieve this goal, Lambert's method is used to calculate the required impulses for each satellite. Lambert's method can be used for this problem, because the positions of each of the four satellites are known for P_1 and P_2, and the time between the two orbital stations is known, because T-frame motion is determined solely by the natural dynamics. The satellites are not controlled during the transit from P_1 to P_2. The same methodology is used to calculate the ΔV for the satellites to perfectly reassemble at P_1 in their original configuration. Equation (1) shows the cost function developed for previous work in VRB optimization , which was also adopted for this work:

$$J = w_1\left(\sum_{Q_{R,i}\geq Q_{R,\min}} Q_{R,i}\cdot\Delta t\right) + w_2\left(\sum_{Q_{G,i}\geq Q_{G,\min}} Q_{G,i}\cdot\Delta t\right) + w_3\left(\frac{\Delta V}{T_{\text{obs}}}\right) \tag{1}$$

where w_1, w_2, and w_3 are weighting factors; $Q_{R,\min}$ and $Q_{G,\min}$ are minimum acceptable values of Q_R and Q_G; $Q_{R,i}$ and $Q_{G,i}$ are Q_R and Q_G at station i in the orbit; Δt is the orbit propagation time step; ΔV is the total ΔV applied around the orbit; and T_{obs} is the time of observation per orbit. As will be discussed next, three primary weight combinations are used for this work. One set is optimized over quality factor Q_R only, with weights $w_1 = -1$, $w_2 = 0$, and $w_3 = 0$; a second set minimized fuel use with weight vectors $w_1 = 0$, $w_2 = 0$, and $w_3 = 1$. The final set has $w_1 = -1$, $w_2 = 0$, and $w_3 = 1.3\times 10^{12}$, a compromise scaled to approximately balance fuel and quality factor influences. Note that w_1 is negative because the quality factor is maximized.

Optimization Methods

A host of local minima are present for the MMS mission design problem studied in this work. Although no algorithm is perfect, we attempt to explore a diverse solution space via two very different optimization strategies: a hierarchical algorithm developed in our previous work and a particle swarm optimization approach with evolutionary algorithm heritage. A comparison of results will enable the adoption of the best solution over these two optimization approaches. Both methods are desirable for this problem, because they do not require knowledge of cost-function derivatives. Both are also attractive compared with classical methods, because they examine a large portion of the search space, which reduces the likelihood of becoming trapped at a local minimum.

Hierarchical Optimization

The hierarchical optimization algorithm used in this work performs a multistage search to identify the best solution. Given a coarse search grid, an initial exhaustive search is performed to identify the regions in which local minima might reside. Next, the lowest-cost coarse search design vectors are locally optimized, and the coarse grid is refined until the region in which the local minimum resides is identified. The refinement process iterates until the algorithm is convinced it has found the globally optimal solution. As a check for optimality, the initial coarse grid is shifted and the hierarchical algorithm is again executed, with the coarse grid itself refined until the shifted-grid solution matches its unshifted counterpart. A more detailed description of this method can be found in [10].

As discussed in previous work, the hierarchical method only converges on the global minimum if the search grid is properly selected or may be sufficiently refined. For satellite formation design problems with numerous local minima, changing the weights of the cost function significantly changes the number and locations of local minima, which increases the difficulty in identifying the globally optimal solution. As an example of how minima change as a function of cost-function weights, consider Table 1 [19]. The solution that optimizes only fuel has a separation between burns of almost π rad, whereas the solution that optimizes only the quality factor has a separation of 0.5 rad. These two minima are very different, but both minimize the cost function, given their associated weights. Adding additional search parameters also increases computational complexity substantially.

To manage computational complexity as more variables are added, grid size must be reduced with standard discrete search algorithms. However, when the size of the grid is substantially reduced, local minima may be missed. Thus, we have adopted a second method that more easily scales with increased problem complexity.

Particle Swarm Optimization

Particle swarm optimization (PSO) is a stochastic optimization method that can rapidly explore large regions of the design vector solution space. PSO has been proven to be a reliable method to identify solutions for a variety of different applications [20–22]. Each design variable x_i has a range of $x_i^{\min}$–$x_i^{\max}$, and no constraints are imposed. The amount a variable can change between iterations lies within $v_i^{\min}$–$v_i^{\max}$. The optimization steps are outlined next and illustrated in Fig. 3.

1) Randomly generate the initial population. A predefined number of candidate solutions (particles) and the initial velocity of each particle are randomly generated. The cost of each particle is calculated and a vector containing all n design variable values and the cost for that design vector is created.

2) Compare the cost of particles. The algorithm has a memory of the best location each individual particle has ever occupied. The vector $\boldsymbol{p}_{\mathbf{best},i}$ (where i represents particle number) contains the cost associated with that location and the design variables that represent the location. All $\boldsymbol{p}_{\mathbf{best},i}$ vectors are initialized to be the starting location of each particle. The algorithm also has a memory of the best location any particle has ever occupied. To initialize this vector, the

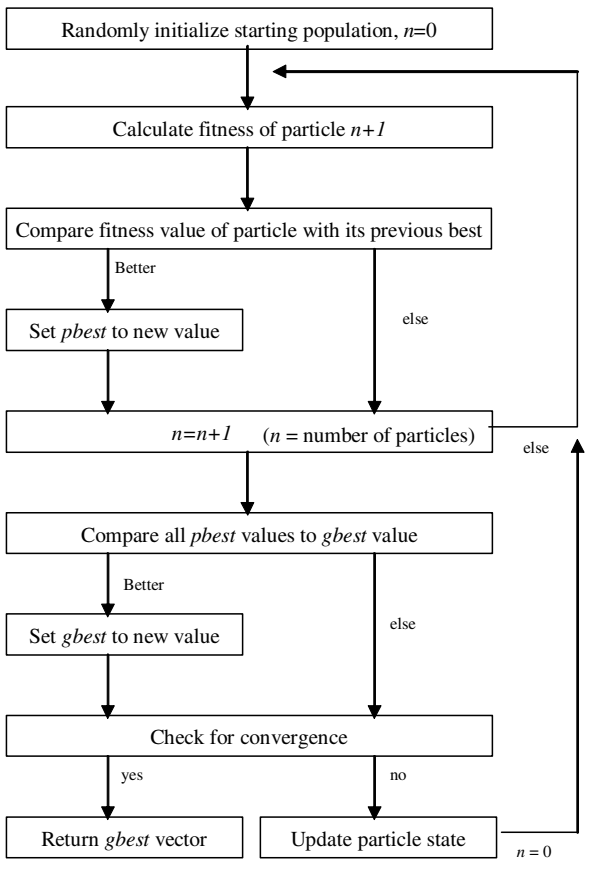

Fig. 3 PSO method.

$\boldsymbol{p}_{\mathbf{best},i}$ vectors are compared and the vector associated with the minimum-cost particle is copied to a vector referred to as $\boldsymbol{g}_{\mathbf{best}}$.

3) Use the iteration process. Equation (2) is used to update the velocity of every particle in every dimension.

$$v_{j+1} = \omega v_j + \frac{c_1 r_1 (p_{\text{best}} - x_j) + c_2 r_2 (g_{\text{best}} - x_j)}{\Delta t} \tag{2}$$

where v_{j+1} is the new velocity, ω is the inertial weight, v_j is the current velocity, c_1 and c_2 are weighting factors, r_1 and r_2 are random factors, p_{best} is the value from the $\boldsymbol{p}_{\mathbf{best},i}$ vector associated with the dimension being updated, x_j is the current position of particle i in dimension j that is being updated, and g_{best} is the value from the $\boldsymbol{g}_{\mathbf{best}}$ vector associated with dimension j. The values of c_1 and c_2 are typically denoted as the cognitive and social parameters, respectively, and can be used to cause the particle to have a tendency to fly past the $\boldsymbol{p}_{\mathbf{best},i}$ and $\boldsymbol{g}_{\mathbf{best}}$ locations. They can also be used to show preference to either the p_{best} or g_{best} term. For this research, all of the c_1 and c_2 values were set to two. This selection allowed the particle to potentially overshoot the best location, a choice that created a varied search pattern. The range of r_1 and r_2 is 0–1. This adds another random element into the problem. The value of Δt is always set to one. The discretization level of ω is selected to trade execution time with result quality; a large value reduces search-space size, but a smaller value results in a more refined search.

After the velocity of a particle is updated in a dimension, the position of that particle in that dimension is also updated via a first-order integration step. After the location for each particle dimension has been computed, particle cost is updated accordingly. The new cost is compared with the previous $\boldsymbol{p}_{\mathbf{best},i}$ cost, and if the new cost compares favorably, $\boldsymbol{p}_{\mathbf{best},i}$ is updated. After all particles are updated for the given iteration, the costs of all of the $\boldsymbol{p}_{\mathbf{best},i}$ vectors are compared with the $\boldsymbol{g}_{\mathbf{best}}$ cost. If a better solution has been found, then $\boldsymbol{g}_{\mathbf{best}}$ is updated.

4) Check the stopping criteria. The PSO process will terminate if either the algorithm has converged to a solution or if the maximum number of iterations is exceeded. If neither condition has been met, step 3 is repeated.

Hierarchical Optimization Versus PSO

The multi-impulse results presented next were obtained using the hierarchical optimization method. The same tests were repeated using the PSO algorithm. The two methods converge to answers with approximately the same cost, with each method outperforming the other in some cases. The PSO algorithm had to be run several times, because there is no guarantee that any single execution of the algorithm will return the global minimum. The hierarchical method is dependent on the initial coarse search grid. Because the number of local minima is not known a priori, this method may also require multiple executions to guarantee that it has found the global minimum. Execution time is also a function of solution convergence rate for both algorithms. As a result, the time needed for each algorithm to find the global minimum is not precisely predictable, but the two methods executed with comparable speed (approximately two days) on a Pentium 4 2.79-GHz desktop machine for the MMS design scenarios described in this paper. The benefit of PSO is that as the search space expands, PSO does not see a significant increase in the amount of time needed to reach convergence, whereas the hierarchical method does.

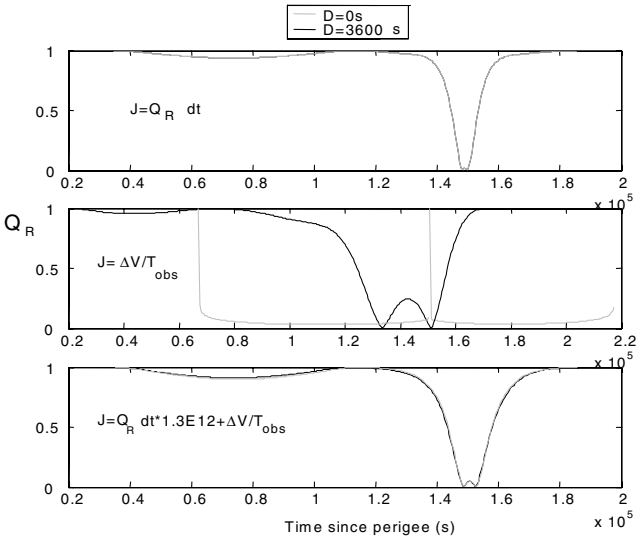

Fig. 4 Single-orbit multi-impulse quality factor evolution.

Multi-Impulse Designs

An initial multi-impulse design strategy derived from VRB results [10] constrained the formation to form a perfect tetrahedron at the two burn locations. The pair of transitions between the two perfect locations was determined by applying Lambert's solution for each transition. The hierarchical optimization algorithm was used to find the minimum-cost solution. In this work, a series of optimizations was performed to evaluate the effects of cost-function weight variations on the solution. Also, to account for disruption in the local magnetic field when thrust is applied, a delay was introduced and assigned one of two values: $D = 0$ (no delay) and $D = 3600$ (observation delay of 1 h after impulsive thrust is applied). We hypothesize that an hour will be an upper bound on delay time, because thruster emissions will disperse and because the spacecraft itself will move away from the disturbed area.

Figure 4 shows the evolution of the quality factor for this series of one-orbit multi-impulse tests, with the T frame as the universal time clock in all plots. Table 1 summarizes the numerical results. All distances are in kilometers and velocities are in kilometers/second. For the Table 1 results, bounds of $\pm 10,000$ km were placed on V_x, V_y, and V_z to enable discovery of optimal solutions further from the T frame reference orbit. For all cost-function weights, as expected, a nonzero D increases cost (i.e., makes cost less negative) by excluding observation regions near the thrust application sites in which the geometry is most perfect. However, the remaining valid observation time per orbit (greater than 80%, for most cases) is still significantly higher than the 34.4% observation time per orbit with the optimized natural orbit solution, identified in previous work [10].

Several conclusions can be drawn from the Table 1 results. First, the optimizer had significant freedom to alter satellite orbits with large V frame offsets. With only $Q\,dt$ cost, a solution was identified

Table 1 Single-orbit multi-impulse solution summary

Input			Solution						Statistics			
Test No.	Cost	Delay	Δv, rad	v_c, rad	$\tilde{\omega}_{\text{true}}$, rad	V_x, km	V_y, km	V_z, km	ΔV/orbit $\sum$ over all sats, km/s	$Q\,dt$ (total)	T_{obs}, %	Cost, J
1	$Q\,dt$	0	0.5132	3.128	8.69E − 04	−9999	9896	−9788	4.23E + 00	134,737.9	92.52	−1.35E + 05
2	$Q\,dt$	1 h	0.5132	3.128	8.69E − 04	−9999	9896	−9788	4.23E + 00	126,744.5	87.21	−1.27E + 05
3	$\Delta V/T_{\text{obs}}$	0	3.1409	1.522	1.10E + 00	−3.71	−14.15	−3.07	2.46E − 10	1999.999	0.66	2.46E − 13
4	$\Delta V/T_{\text{obs}}$	1 h	0.4205	2.917	2.22E − 01	0.08	−4.12	115.9	7.31E − 04	99,147.72	69.30	7.00E − 09
5	Both	0	0.5045	3.130	2.30E − 02	−0.36	50.55	−208.7	9.6E − 04	124,945.1	87.21	−1.15*E* + 05
6	Both	1 h	0.5258	3.137	6.38E − 03	0.61	−1.68	332.3	9.83E − 04	117,051.9	82.24	−1.07*E* + 05

that allowed the formation to use large offsets to better align satellites across the drift periods. These $Q\,dt$ solutions (tests 1 and 2) are not attractive, however, because of the significant ΔV required. Perhaps the most surprising result was achieved in test 3 ($\Delta V/T_{\text{obs}}$ cost, no delay). Because quality is not included in the cost function, the optimizer chose a solution that met the constraint of "perfect geometry at impulse sites," but the formation immediately diverged from a tetrahedron, due to the out-of-plane satellite 4 orbit. This solution is not acceptable from a quality factor perspective, but the optimizer did its job, requiring a ΔV that was many orders of magnitude less than other solutions.

Test 4 ($\Delta V/T_{\text{obs}}$ cost and $D = 1$ h) could not adopt the low-fuel result from test 3, because no region with $Q_R > 0.7$ was present outside the area contaminated by thruster use (i.e., $T_{\text{obs}} = 0$). An alternate solution was identified that required significantly more fuel, but had nonzero observation time. This solution is similar to results that include $Q\,dt$ cost, but with a somewhat lower integrated quality factor and ΔV. The most promising one-orbit multi-impulse solution, tests 5 and 6 in Table 1, uses the cost function with both fuel use and quality factor terms. With no delay, observation can occur over 87% of the orbit with reasonable fuel use; with delay, a comparable solution is found, but observation time (82%) is reduced by the delay period following thruster use.

Formation-Attitude Two-Body Results

Because of the added complexity of the search space due to the inclusion of new variables that describe the formation attitude, only the PSO algorithm was used to solve this problem. The search space for this problem consisted of $\Delta\nu$, ν_c, V_x, V_y, V_z, and two sets of XYZ Euler angles; one set of angles describes the formation attitude at P_1 and the other set describes the formation attitude at P_2. The best solution had $\Delta\nu = 0.4567$ rad; $\nu_c = 3.0944$ rad; $\boldsymbol{V} = 1.1217$, -16.0349, and -99.9574 km; and XYZ Euler orientations 0.1793, -0.1516, and 0.3045 rad for P_1 and -0.4066, 0.3174, and 0.2880 rad for P_2. The $\boldsymbol{V}$ offset vector, in combination with the respective rotation set, defines the offset from the T frame at P_1 and P_2. Formation geometry snapshots at P_1 and P_2, as well as apogee and perigee, are illustrated in Fig. 5. Our optimal solution indicates that close proximity to the T-frame x axis is more critical than for y and z. Because the semimajor axis of the T frame is coincident with the x axis, it is logical that distance from the x axis should be minimized, because separation from the T frame x axis causes a change in natural orbital period that must be corrected. This same trend was observed with the optimal solution to the default formation-attitude problem; a more detailed explanation is provided in [19,23]. The results indicated a linear relationship between V_x and V_y.

The inclusion of formation attitude in our design vector has decreased solution cost compared with previous results; the default formation-attitude solution had a total cost of -1.07×10^5 using Eq. (1) with $w_1 = -1$, $w_2 = 0$, and $w_3 = 1.3 \times 10^{12}$. The attitude-optimal solution has a total cost of -1.15×10^5 using the same cost-function weights, a 9% decrease in cost. The total ΔV summed over all satellites is 8.63×10^{-4} km/s per orbit for the attitude-optimal solution, a 12% decrease relative to the default formation-attitude solution. Table 2 summarizes the default formation attitude and attitude-optimal results, and Fig. 6 provides a comparison of quality factor Q_R over a full orbit. Note that although the quality factor for our new solution is less than the default formation-attitude quality for an interval after P_2, optimizing over attitude has improved quality around apogee, the point at which data would mostly likely be collected. In summary, the attitude-optimal solution has improved the default attitude solution with respect to both quality and required fuel expenditure.

Table 2 Comparison of two-body default formation-attitude and attitude-optimal solutions

	Default attitude	Attitude optimal
Cost	−1.07E + 05	−1.15E + 05
Total ΔV, km/s	9.83E − 04	8.75E − 04
T_{obs}, %	82.2	86.2
Average Q	0.9440	0.9531

To study the nature of the minima, we exploit the fact that PSO, like other evolutionary algorithms, cannot guarantee that the globally best solution is always found. A set of 153 candidate solutions near the apparent global minima (cost $\leq 1.15 \times 10^5$) were identified for the 488 PSO optimization processes. The selection of $\Delta\nu$, ν_c, and V_z has been previously explained [19]. The parameter $\Delta\nu$ is selected to allow the two burns to occur near apogee. The exact value determines how low the quality factor will be at apogee. The parameter $\Delta\nu$ centers P_1 and P_2 approximately near apogee. V_y and V_z appear randomly distributed; however, the value of V_x does appear to depend on the value of V_y. All Euler angle rotations were searched over an interval of ± 0.5236 rad (± 30 deg), and so we conclude that the values were not influenced by search-space boundaries. P_1 and P_2 have noticeably different formation attitudes. For a positive z rotation at P_1, satellite 3 is rotated so that its unit vector is primarily along the V-frame x axis. Satellites 1 and 4 have the same basic relationship with the y and z axes, respectively. Because of the geometry and the other three satellites' proximity to the axes, satellite 2 is approximately equidistant from the x and y axes; it is also the only one of the four satellites with a negative z component. The rotation of the formation about the z axis is approximately equal at both orbital stations. The z axis rotation at P_1 is close to equal to the z axis rotation at P_2. The few negative rotation solutions are near the search-space boundary and are removed from the data set for analysis. Boundary data are more likely to be a local minimum, so we focus analysis on positive-z-rotation solutions. The rotation about the z axis effectively causes a change in the value of $\tilde{\omega}_{\text{true}}$ for the

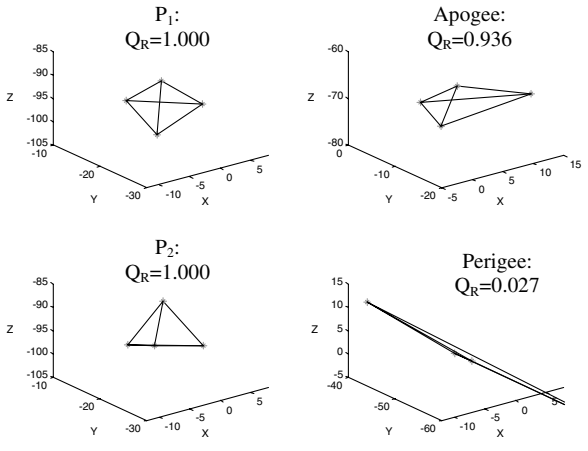

Fig. 5 MMS geometry at varied orbital stations.

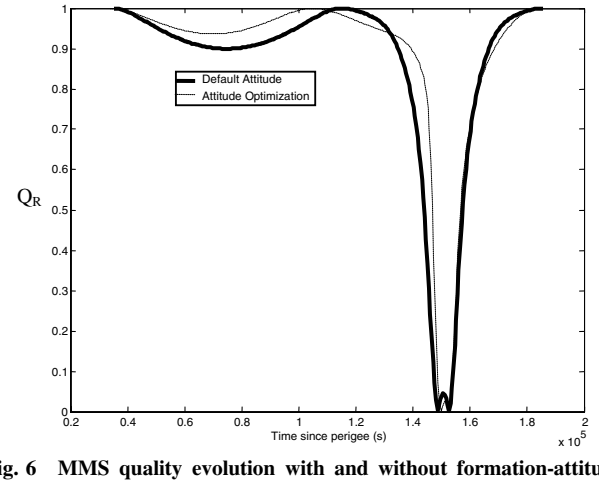

Fig. 6 MMS quality evolution with and without formation-attitude optimization.

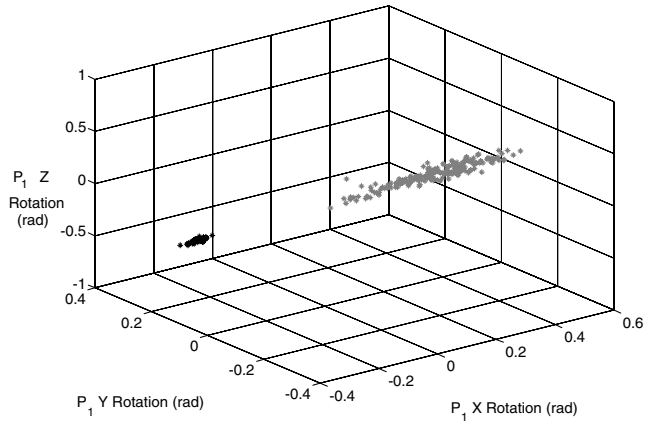

Fig. 7 P_1 rotation angles.

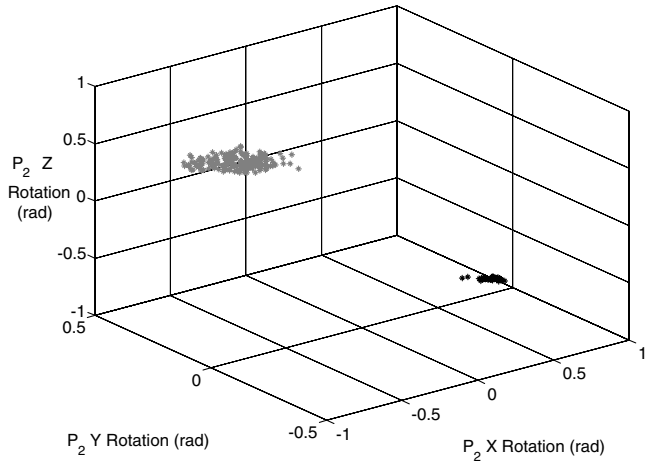

Fig. 8 P_2 rotation angles.

transfer orbit. A node change at the burn site would increase the amount of needed fuel.

Figures 7 and 8 illustrate the rotation angles at P_1 and P_2, respectively, for the candidate solutions close (within 0.15%) to the best solution. Two clusters appear in the plots, because of the symmetry of the formation. If the bounds of the search space were altered slightly, then the cluster in the negative z region of the plots would be found at in the positive z region. The transit from P_1 to P_2 is near apogee and the satellites are moving relatively slowly, compared with their orbital speed. The rotation specified at P_1 for the lowest-cost solution aligns the formation more closely with the motion of the target orbit. By rotating the formation so that it is more closely aligned with the path of the target orbit, the quality factor increases, because the satellite orbits are more similar.

In comparison, the transition from P_2 to P_1 will not provide as good of an opportunity to collect data, because even slight differences in satellite orbits will cause the formation to degrade significantly, given the high orbit velocities near perigee. Because the quality factor and observation time will be insignificant, the dominant cost-function term for the P_2–P_1 transit is fuel. If a satellite is on the target orbit, it incurs minimal fuel cost, because it will naturally arrive at P_1 with the same velocity as the target frame. It is not possible to place all four satellites on the target orbit and have a quality factor of one at P_2 (or P_1). However, the rotations at P_2 place the three in-plane satellites approximately on the target orbit, thereby minimizing fuel cost.

As illustrated by the Fig. 5 perigee plot, formation satellites may travel quite close to each other over the drift orbit. We incorporated a collision avoidance check in our optimization process to eliminate any solution that is infeasible due to potential satellite collision. However, by removing solutions with collision potential, PSO clustering/convergence performance was reduced. Because PSO convergence degraded with the inclusion of a collision check, it was removed from the optimization process. However, postprocessing of the optimal solution determined that the closest approach of any two satellites in our lowest-cost solution is greater than 1.25 km. We have elected to postprocess the final solution, and if a future solution is found in which a collision might occur, then the optimization will be rerun that includes the collision check. This procedure allows PSO to perform efficiently and still guarantee that our final solution will be collision-free.

Perturbation Results

The assumption that the only forces acting on the satellites are the Keplerian two-body forces allowed us to efficiently identify candidate MMS designs. Both the PSO and hierarchical methods investigate millions of solutions for each design problem; without the Keplerian assumption, computation time would be prohibitive. However, the perturbing forces are not insignificant and must be taken into consideration for the final design. A simulator [9] that includes lunar perturbations, atmospheric drag, and the J_2–J_5 forces was applied to the baseline MMS design obtained in test 6 (Table 1). The simulator we chose does not include all possible perturbations; most notably, solar pressure and solar gravitation are ignored. However, the use of preexisting software was deemed an acceptable trade-off, because the perturbations were primarily included to validate results. The baseline solution previously described was selected for this analysis, because it was observed to provide balance between quality and fuel use, as well as to conservatively model data-collection interruption near impulse application sites.

The formation was initially placed at orbital station P_1 (in its configuration from Fig. 2), and the velocity of each satellite was set to the velocity that had been determined using Lambert's method to set up the next drift-orbit segment. At orbital station P_2, the velocities of the satellites were adjusted so that they were the values determined using Lambert's method. As shown in Table 3, a position error (Δx, Δy, or Δz) between the estimated two-body solution and the simulator results exists. The required ΔV is significantly higher than the previously calculated values. The first three columns in Table 3 show differences in positions, the next three columns contain the ΔV

Table 3 First orbit perturbed simulation results

P_1	Δx, km	Δy, km	Δz, km	Lambert ΔV_x, km/s	Lambert ΔV_y, km/s	Lambert ΔV_z, km/s	Simulation ΔV_x, km/s	Simulation ΔV_y, km/s	Simulation ΔV_z, km/s
S1	−6.82	116.28	−3.88	0.00E + 00	0.00E + 00	0.00E + 00	2.03E − 03	2.05E − 03	2.31E − 04
S2	−6.86	116.29	−3.88	−1.86E − 04	−1.63E − 04	1.00E − 06	2.21E − 03	1.89E − 03	2.30E − 04
S3	−6.91	116.08	−3.88	1.85E − 04	1.62E − 04	−1.00E − 06	1.85E − 03	2.21E − 03	2.32E − 04
S4	−6.83	116.26	−3.92	−2.00E − 06	−1.00E − 06	0.00E + 00	2.03E − 03	2.05E − 03	2.31E − 04
P_2									
S1	52.92	17.83	9.80	0.00E + 00	0.00E + 00	0.00E + 00	1.84E − 03	5.43E − 04	2.20E − 04
S2	53.01	17.81	9.83	−1.81E − 04	1.63E − 04	1.00E − 06	2.03E − 03	7.07E − 04	2.19E − 04
S3	52.99	17.82	9.79	1.80E − 04	−1.62E − 04	−1.00E − 06	1.66E − 03	3.81E − 04	2.20E − 04
S4	52.94	17.82	9.81	−1.00E − 06	1.00E − 06	0.00E + 00	1.85E − 03	5.45E − 04	2.19E − 04
Total ΔV, km/s				Lambert = 9.83E − 04			Simulation = 1.94E − 02		

Table 4 Position error and ΔV with iteration

P_1	Δx	Δy	Δz	ΔV_x	ΔV_y	ΔV_z	Total ΔV
S1	−0.01	−1.50	−0.06	2.16E − 03	1.74E − 03	2.21E − 04	2.79E − 03
S2	0.00	−1.52	−0.05	2.35E − 03	1.58E − 03	2.20E − 04	2.84E − 03
S3	0.02	−1.48	−0.05	1.98E − 03	1.90E − 03	2.21E − 04	2.76E − 03
S4	−0.01	−1.50	−0.02	2.17E − 03	1.74E − 03	2.20E − 04	2.79E − 03
P_2							
S1	0.04	0.00	0.01	8.87E − 04	4.89E − 04	2.91E − 04	1.05E − 03
S2	−0.04	0.01	−0.01	1.07E − 03	6.51E − 04	2.91E − 04	1.29E − 03
S3	−0.02	0.00	0.03	7.01E − 04	3.26E − 04	2.92E − 04	8.27E − 04
S4	0.02	0.01	0.00	8.88E − 04	4.90E − 04	2.92E − 04	1.06E − 03

Table 5 Perturbation error and ΔV after iteration for the attitude-optimal solution

P_1	Δx, km	Δy, km	Δz, km	Δr, km	ΔV_x, km/s	ΔV_y, km/s	ΔV_z, km/s	ΔV, km/s	ΔV Kep opt, km/s
S1	−0.11	−1.67	−0.05	1.67	1.71E − 03	2.04E − 03	1.62E − 04	2.67E − 03	1.60E − 11
S2	−1.38	−2.06	−0.09	2.48	1.82E − 03	1.95E − 03	1.63E − 04	2.67E − 03	1.04E − 04
S3	−0.22	−1.63	−0.05	1.65	1.53E − 03	2.26E − 03	1.62E − 04	2.74E − 03	3.70E − 04
S4	−0.22	−1.67	−0.07	1.68	1.72E − 03	2.03E − 03	1.62E − 04	2.67E − 03	9.05E − 12
P_2									
S1	0.03	0.01	0.00	0.04	3.21E − 03	−8.98E − 04	3.18E − 04	3.35E − 03	1.31E − 11
S2	0.02	−0.02	0.01	0.03	3.31E − 03	−8.31E − 04	3.17E − 04	3.43E − 03	8.85E − 05
S3	0.02	−0.01	−0.01	0.03	2.91E − 03	−1.10E − 03	3.18E − 04	3.13E − 03	3.03E − 04
S4	0.02	0.02	0.03	0.04	3.21E − 03	−8.97E − 04	3.18E − 04	3.35E − 03	7.42E − 12

Table 6 MMS design comparison

	Keplerian solution	Perturbed Kep solution	Iterated pert of Kep solution	Perturbed Kep solution using SDP4
Cost	−1.07E + 05	-	-	-
Total ΔV, km/s	9.83E − 04	1.94E − 02	1.54E − 02	2.46E − 03
T_{obs}, %	82.2	82.1	82.2	81.9
Average Q	0.9440	0.9440	0.9395	0.9448

calculated using Lambert's method, and the final columns list the ΔV that the simulator applied to achieve the desired velocities (given the Keplerian design) at orbital stations P_1 and P_2.[‡]

Even though there is a change in the position and the required ΔV, the formation geometry does not change during the orbit, relative to the initial estimated solution. The assumption had been made that the satellites would return to the initial positions once per orbit. However, as was shown in our previous work [23], the perturbations disallow that assumption.

To correct the position error caused by the perturbing forces, the simulator is executed with the two-body conditions for transit from P_1 to P_2. The desired positions of the satellites are P^D_{2j}. However, due to the perturbing forces, the satellites actually occupy positions $P^A_{2,j}$ ($j = 1, 2, 3$, and 4 for all MMS satellites). The position error ΔP_{2j} is calculated from

$$\Delta P_{2,j} = P^A_{2,j} - P^D_{2,j} \tag{3}$$

The new target point is then set to

$$P^*_{2,j} = P^D_{2,j} - \Delta P_{2,j} \tag{4}$$

Lambert's method is used to solve for the ΔV needed to go from P_1 to $P^*_{2,j}$. We are therefore making the assumption that the error will be approximately the same as with the initial conditions. Table 4 illustrates the magnitude of position error resulting from this iteration scheme. The process is repeated for the transit through perigee from P_2 to P_1. A comparison of Table 3 with Table 4 shows that the reduction in position error relative to the two-body reference orbit also results in a decrease in required ΔV. This process could be repeated to further reduce position error, thereby further reducing the ΔV. However, the savings will not be nearly as significant for additional iterations. The same iteration scheme was used to evaluate the influence that perturbations would have on the attitude-optimal solution, and results are provided in Table 5.

For this analysis, the simulator is used as a postprocessing step, because of the computational time required for a single propagation. Although the preceding iteration scheme returns the satellites to approximately the same location after each orbit, there is a substantial increase in the required amount of fuel, which ultimately must be factored into the mission optimization process. The significant increase in required ΔV might, at first, cast doubt on the two-body results. However, in previous work [23], we showed that the amount of total ΔV can be reduced if the T frame and the satellites are both propagated with perturbations, instead of only the satellites being perturbed, with the T frame being propagated with a two-body model. The question that remains is whether inclusion of perturbing forces in the optimization algorithm significantly changes the solution. A summary of the perturbation analysis is provided in Table 6.

The two-body results required very little fuel, because spacecraft were on transfer orbits that follow a target orbit with the same force model. In the simulation results, satellites were influenced by perturbing forces but attempted to follow an orbit propagated without these forces. Therefore, we hypothesized that a significant reduction in fuel could be achieved if the T frame orbit was propagated using the same perturbing forces used to propagate the satellites.

To determine the amount of associated fuel reduction, we used a simplified deep-space generalized-perturbations (SDP4) function of the SGP library [24] to propagate both the T frame and the satellites for our baseline solution. Results are presented in Table 6. There is an increase in the total amount of fuel required relative to two-body results, because of the perturbing forces, but the amount of fuel is

[‡]Velocities varied significantly after each drift period, and it was observed that the quality factor degraded to near zero after the first burn at P_1 when velocities were not matched with those identified during the Keplerian optimization process.

now a factor of 2.5 greater than that required by the baseline solution. We expect further improvement will be possible in future work through use of SDP4 during optimization.

Conclusions

Hierarchical and particle swarm optimization methods were applied to design a four-satellite tetrahedral formation in an elliptical geocentric orbit. As a compromise between purely natural and continuously controlled strategies, this paper investigates multi-impulse formation designs in which low-magnitude impulses are applied at specific orbital stations to maximize formation quality over a full orbit. We have studied a variety of multi-impulse designs applicable to the MMS mission, presuming perfect geometry at impulse application sites. We introduced a delay parameter to account for disturbances to the magnetic field following thruster use.

Hierarchical optimization provides a structured way to uniformly search or focus efforts on a specific part of the design vector space when the nature of local minima is known to some extent. However, to obtain accurate results without knowledge of minima region location or size, the search space must often be refined such that large problems are infeasible to optimize. Although multiple iterations are required, given its stochastic nature, PSO scales more readily to large optimization problems without the same computational penalty. In terms of solution quality, both optimization methods find similar solutions that are comparable in cost, and multiple PSO trials are used to improve statistical completeness.

We have investigated multi-impulse mission designs for a tetrahedron formation optimized over attitude, as well as thrust application sites, and offset from a reference orbit. The results show an improvement in cost (quality of observation, amount of fuel, and observation time) for the two-body solution over our initial solution that presumes a fixed formation attitude at impulse application sites. Perturbations influence the cost of the final solution, but if all satellites, real and virtual, are controlled by the same dynamics, then the increase in cost due to perturbations is more reasonable than when one component is influenced by perturbations and the other is not. To include perturbations in the general optimization process, analytical methods must be used for computation time to be manageable. These methods are not as exact as numerical integration, but they provide a reasonable estimate. Future work will be required to develop a perturbed Lambert's method that will reliably converge on the true optimal solution, given perturbations.

One of the assumptions made for this work is that a single orbit is repeated. However, the method we have implemented to include perturbations does not guarantee that the formation will precisely return to P_1 for reassembly. In fact, the perturbing forces change for each orbit, and so it is not likely to find an exact repeatable orbit that meets the mission requirements. We could use a perturbed Lambert's algorithm to find an orbit that passes through P_1 twice, separated by the desired orbital period. P_2 would be calculated the same way as it is currently for the perturbed case: the time would be calculated based on two-body dynamics, and then the orbit would be propagated over that time period.

Although adjusted to balance fuel use and quality factor, relative cost-function weights were tuned manually for this paper. The PSO software can be expanded to handle multiple objectives through determination of the Pareto frontier [25]. This information gives the mission designer a set of candidate solutions with different relative weights, without repeated runs of each optimization tool. The optimal formation-attitude results indicated that locations P_1 and P_2 serve different roles and therefore have different optimal formation attitudes. The optimal values of V_x, V_y, and V_z could be different at the two locations, and so a logical next step would be to include a second set of offsets in the optimization process.

Acknowledgments

This work was partially supported under NASA Goddard Space Flight Center grant NNG04GA64A. The authors would like to thank Liam Healy, Rob Sanner, and Steve Hughes for their invaluable feedback. We also thank Daniel Chavez-Clemente for his contributions on the hierarchical optimization software, as well as on the virtual rigid body and natural orbit Magnetospheric Multiscale mission design formulations upon which this work was built. We would also like to thank Rob Sanner for his development of the perturbation simulation code.

References

[1] Conkey, D., Dell, G., Good, S., and Bristow, J., "EO-1 Formation Flying Using Autocon^{TM}," *Proceedings of the IEEE Aerospace Conference*, Vol. 7, Institute of Electrical and Electronics Engineers, Los Alamitos, CA, 2000, pp. 55–61.

[2] DeCou, A. B., "Orbital Station-Keeping for Multiple Spacecraft Interferometry," *Journal of the Astronautical Sciences*, Vol. 39, No. 3, July–Sept. 1991, pp. 283–297.

[3] Hadaegh, F. Y., Lu, W.-M., and Wang, P. K. C., "Adaptive Control of Formation Flying Spacecraft for Interferometry," *Large Scale Systems: Theory and Applications (IFAC 1998)*, Pergamon, Oxford, England, U. K., 1998.

[4] Siegel, A., and Blandino, J., "Propulsion Requirements and Options for Astronomical Imaging Formations in Earth Orbit," 39th AIAA/ASME/SAE/ASEE Joint Propulsion Conference, AIAA Paper 2003-4577, 2003.

[5] Vassar, R. H., and Sherwood, R. B., "Formation Keeping for a Pair of Satellites in a Circular Orbit," *Journal of Guidance, Control, and Dynamics*, Vol. 8, Mar.–Apr. 1985, pp. 235–242.

[6] Inalhan, Gökhan, Tillerson, Michael, and How, Jonathan, P., "Relative Dynamics and Control of Spacecraft Formations in Eccentric Orbits," *Journal of Guidance, Control, and Dynamics*, Vol. 25, No. 1, Jan.–Feb. 2002, pp. 48–59.

[7] Ren, W., and Beard, R., "Decentralized Scheme for Spacecraft Formation Flying Via the Virtual Structure Approach," *Journal of Guidance, Control, and Dynamics*, Vol. 27, No. 1, Jan.–Feb. 2004, pp. 73–82.

[8] Campbell, M., and Schetter, T., "Comparison of Multiple Agent-Based Organizations for Satellite Constellations," *Journal of Spacecraft and Rockets*, Vol. 39, No. 2, Mar.–Apr. 2002, pp. 274–282.

[9] Penneçot, Y., Atkins, E., and Sanner, R., "Intelligent Spacecraft Formation Management and Path Planning," Aerospace Sciences Meeting and Exhibit, Reno, NV, AIAA Paper 2002-1072, 2002.

[10] Chavez-Clemente, D., and Atkins, E., "Optimization of Tetrahedral Satellite Formations," *Journal of Spacecraft and Rockets*, Vol. 42, No. 5, July–Aug. 2005, pp. 699–710.

[11] Curtis, S., "The Magnetospheric Multiscale Mission...Resolving Fundamental Processes in Space Plasmas," NASA Goddard Space Flight Center Rept. TM2000-209883, Greenbelt, MD, 2000.

[12] Curtis, S., Petruzzo, C., Clark, P., and Peterson, A., "The Magnetospheric Multi-Scale Mission: An Electronically Tethered Constellation Of Four Spacecraft," *Third International Workshop on Satellite Constellations and Formation Flying*, 2003.

[13] Hughes, S. P., "Formation Tetrahedron Design for Phase I of the Magnetospheric Multiscale Mission," *Proceedings of the Flight Mechanics Symposium*, NASA Goddard Space Flight Center, Greenbelt, MD, 2003.

[14] Hughes, S. P., "Orbit Design for Phase I and II of the Magnetospheric Multiscale Mission," *AAS 27th Rocky Mountain Guidance and Control Conference*, American Astronautical Society, San Diego, CA, 2004.

[15] Williams, Trevor, Register, Justin, and Slater, Gary, "Formation-Keeping Maneuver Dispersions and Safe Mode Insertion for Satellite Formation Flight," AIAA Guidance, Navigation and Control Conference, AIAA Paper 2004-4734, 2004.

[16] Gim, Dong-Woo, and Alfriend, Kyle, T., "The State Transition Matrix of Relative Motion for the Perturbed Non-Circular Reference Orbit," *Journal of Guidance, Control, and Dynamics*, Vol. 26, No. 6, Nov.–Dec. 2003, pp. 956–971.

[17] Schweighart, Samuel, A., and Sedwick Raymond, J., "High-Fidelity Linearized J2 Model for Satellite Formation Flight," *Journal of Guidance, Control, and Dynamics*, Vol. 25, No. 6, Nov.–Dec. 2002, pp. 1073–1080.

[18] Robert, P., Roux, A., Harvey, C., Dunlop, M., Daly, P., and Glassmeier, K.-H., "Tetrahedron Geometric Factors," in *Analysis Methods for Multi-Spacecraft Data*, edited by G. Paschmann and P. W. Daly, ESA Publications Div., Noordwijk, The Netherlands, 1998, Chap. 13, pp. 323–348; also International Space Science Inst. Rept. SR-001.

[19] Hoskins, A., and Atkins, E., "Spacecraft Formation Optimization with a Multi-Impulse Design," AIAA Guidance, Navigation and Control Conference, AIAA Paper 2005-5835, 2005.

[20] Eberhart, R. C., and Kennedy, J., "A New Optimizer Using Particle Swarm Theory," *Proceedings of the Sixth International Symposium on Micromachine and Human Science*, Inst. of Electrical and Electronics Engineers, New York, 1995, pp. 39–43

[21] He, S., Prempain, E., and Wu, Q. H., "An Improved Particle Swarm Optimizer For Mechanical Design Optimization Problems," *Engineering Optimization*, Vol. 36, No. 5, 2004, pp. 585–605.

[22] Venter, G., and Sobieszczanski-Sobieski, J., "Multidisciplinary Optimization of a Transport Aircraft Wing Using Particle Swarm Optimization," *Structural and Multidisciplinary Optimization*, Vol. 26, Nos. 1–2, Jan. 2004, pp. 121–131.

[23] Hoskins, A., and Atkins, E., "Formation Attitude Optimization with a Multi-Impulse Design," *Proceedings of the Flight Mechanics Symposium*, NASA Goddard Space Flight Center, Greenbelt, MD, 2005.

[24] Hoots, Felix, R., and Roehrich, Ronald, L., "Models for Propagation of NORAD Element Sets," *Spacetrack Report No. 3* [online archive], http://celestrak.com/NORAD/documentation/spacetrk.pdf [retrieved 8 Aug. 2005].

[25] Hoskins, A., and Atkins, E., "Satellite Formation Design with a Multi-Objective Optimization Technique," AIAA/AAS Astrodynamics Specialist Conference, AIAA Paper 2006-6013, 2006.

C. McLaughlin
Associate Editor